WARSAW UNIVERSITY OF TECHNOLOGY | Index 351733
FACULTY OF CIVIL ENGINEERING
COMMITTEE FOR CIVIL AND WATER ENGINEERING
POLISH ACADEMY OF SCIENCES | ISSN 1230-2945

DOI: 10.24425/ace.2026.1400

ARCHIVES OF CIVIL ENGINEERING

Vol. LXXII ISSUE 3 2026

pp. 401 –416

Research paper

Collaborative working mechanism and seismic effect analysis of assembled sandwich shear walls connected by double row reinforcing bars

Haiting Lu[1]

Abstract: To achieve the equivalent connection between cast-in-place and post poured prefabricated sandwich shear walls, a reinforced post poured double row dowel connection method suitable for prefabricated sandwich shear walls is proposed. This method compares and analyzes shear wall specimens with cast-in-place, reinforced wet and unreinforced wet connections through quasi-static tests, to achieve the coordinated work of the inner and outer leaf walls of sandwich shear walls and improve their seismic performance. The peak load of specimen PS-1 was 3.56 times the cracking load, and its failure load displacement was 15.6 mm more than the peak load displacement. The energy dissipation coefficients under cracking, peak, and failure loads were 0.366, 0.557, and 0.940, respectively. The displacement of specimen WS-1 with reinforced wet connection after pouring was 1.78 times that of the peak load displacement when it reached the failure state. The energy dissipation coefficients under cracking, peak load, and failure load were 0.366, 0.557, and 0.940, respectively. The proposed sandwich shear wall connection method institute has excellent seismic performance and practical application value in high seismic intensity areas.

Keywords: double row reinforcing bars, connection method, sandwich shear wall, collaborative work, seismic performance

[1]PhD., Department of Architectural Engineering, Fushun Vocational Technology Institute, Fushun 113122, China, e-mail: luhaiting0112@126.com, ORCID: 0009-0009-4353-9528

1. Introduction

In recent years, the introduction of low-carbon living, energy conservation and emission reduction, and green building policies has led to the vigorous promotion of Prefabricated Buildings (PB) [1]. Compared with traditional Cast-In-Place (CIP) structures, PB can improve building quality, effectively shorten construction period, and save energy [2]. With the development of construction engineering, Prefabricated Shear Wall (PSW) prefabricated components have been widely studied and applied in the seismic performance research of modern buildings. However, in areas with high seismic intensity, due to a shortage of technical expertise, the collapse of masonry and civil structures during earthquakes is very serious. Therefore, the study of seismic performance of PSW components is of great significance [3, 4]. PSW made of precast concrete or steel can provide excellent lateral support in buildings and effectively resist the influence of natural forces such as earthquake and wind pressure on buildings [5]. However, the existing PSW connection method is not effective in earthquake resistance, leading to the phenomenon of building collapse. Therefore, to enhance the stability of the structure, and improve the construction efficiency of the building project, it is urgent to conduct improved design research on the connection method of PSW [6].

PB is a popular assembly structure system in current applications, and scholars have conducted extensive research on its related applications. Curkovic et al. proposed a composite system combining cold-formed steel components with concrete to investigate the performance of component connection methods. This method achieved composite pin rib connection through shear connection between bolts and corrugated web plates of steel beams, which could ensure high shear strength while reducing ductility [7]. Shen et al. built a PB observation system, which could effectively improve the safety risk management of PB construction [8]. Wang et al. explored the strategies for reducing carbon emissions in PB component manufacturing from the perspective of PB component manufacturing. Low carbon production cost and production efficiency were the main factors affecting the use of low-carbon production technology by PB component production enterprises, providing effective ways and suggestions for the development of low-carbon economy [9]. Xiao et al. studied the alkali activated precast building recycled concrete for foam light soil, and characterized its structure by scanning electron microscope and infrared spectrum. The flowability of this structure was 174 mm, the water absorption rate was 23.16%, and the strength was 1.53 MPa [10]. Zhao et al. proposed an intelligent control method for prefabricated component lifting based on the Internet, which used remote radio technology to collect and transmit data. The proposed method could optimize the lifting process of prefabricated components [11]. Han et al. developed an evaluation method for carbon emissions and established a carbon emission model. The carbon emissions of PB was more than traditional CIP buildings, and the prefabricated components significantly reduced carbon emissions [12].

Prefabricated Sandwich Shear Wall (PSSW) is popular in practical applications of construction engineering due to its low manufacturing cost and good composite performance. Zhao et al. investigated the damage process and damage mode of PSSW by studying the shear resistance of connectors combining stainless steel and glass fiber. Among them, the influence of joint diameter and joint number ratio was more significant [13]. Liu et al. investigated the seismic performance of a new type of PSSW, mainly by designing shear wall specimens for testing. The seismic performance indicators of the components were similar, and the ductility of the specimens was low. Prefabricated components had little influence on the seismic performance of the structure [14]. Tawil et al. optimized the shear performance of S-type PSSW. An analysis was conducted on the insulation thickness and stiffness of S-type connectors. Under certain parameter conditions, the S-shaped shear connector reached its maximum secant stiffness [15]. Xu et al. analyzed the seismic performance and vulnerability of PSSW structures. Reasonable specimens and prefabricated structures could achieve better ductility, stiffness, and energy dissipation capacity. Its application could save material consumption and improve assembly efficiency [16]. Chen et al. studied the shear capability of PSSW connectors and analyzed the failure modes, failure loads, and other indicators. The mean shear bearing capacity of the component in question was 8.37 kN, and its shear performance and ductility were relatively commendable [17].

In summary, the connection method of PSSW has been widely studied and applied. However, in areas with high seismic intensity, existing technologies and shear wall connection methods cannot effectively resist earthquakes, and their practicality is poor. Therefore, this study proposes an equivalent CIP connection method suitable for PSSW, which combines CIP and precast CIP. By comparing different connection methods of sandwich shear walls through quasi-static experiments, the collaborative working mechanism and seismic effect of the inner and outer leaf walls of double row reinforced shear walls are explored, to achieve equivalent connection effects of post pouring wet connection and CIP connection of double row reinforced shear walls.

The innovation of the research lies in the design of a reinforced wet connection specimen suitable for PSSW, which not only achieves "equivalent CIP" but also improves seismic resistance, providing reference for practical applications in high-frequency earthquake areas.

2. Methods and materials

This section first improves the cast-in-situ shear wall connected by single row dowel bars and designs its specimens. Then, a reinforced wet sandwich shear wall specimen based on double row dowel bar connection is designed to achieve the equivalent connection effect of CIP.

2.1. Design of CPSSW specimens based on improved single row plug-in connection

The connection technology of shear wall is the core to distinguish the precast and CIP concrete structures. The failure of the connection point may lead to the destruction and collapse of the whole shear wall structure [18]. The quality and seismic performance of shear wall components with traditional single row reinforcing bar connections are poor. In this study, a Cast-in-place Sandwich Shear Wall (CPSSW) specimen with Double Row Reinforcing Bar Connection (DRRBC) is designed, and the failure phenomenon, ductility, and energy dissipation capacity of DRRBC's CPSSW and solid shear wall are compared and analyzed through quasi-static tests to explore the collaborative working mechanism of the inner and outer leaf walls of the sandwich shear wall. Two wall specimens were designed for the experiment, and the parameter design and detailed construction of the specimens are shown in Fig. 1. PS-1 is the CPSSW specimen of DRRBC, and PS-2 is the solid shear wall specimen of DRRBC.

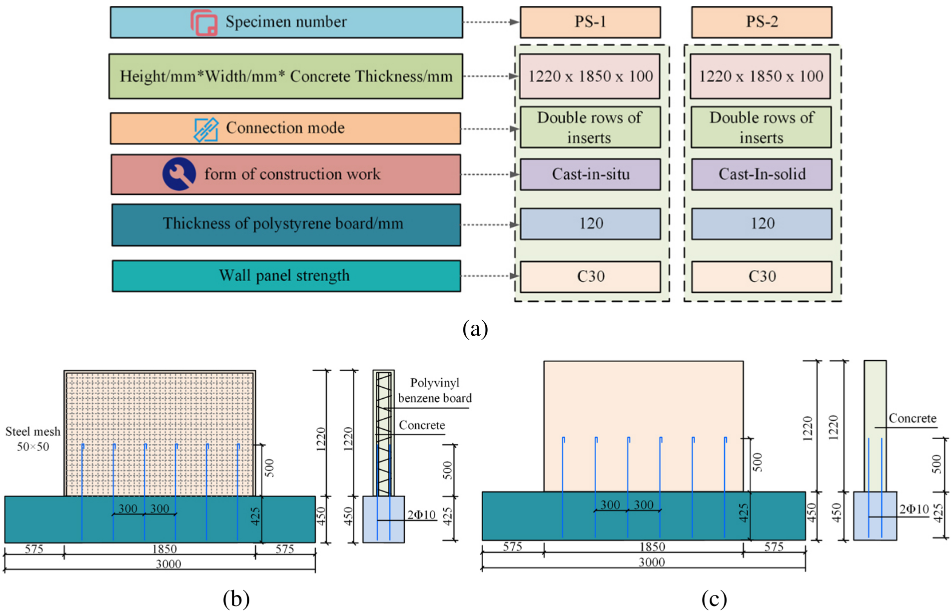

Fig. 1. Cast-in-situ shear wall specimen design parameters and detailed structure diagram; (a) Parameters of cast-in-place shear wall specimen, (b) Detailed construction diagram of PS-1, (c) Detailed construction diagram of PS-2

Following the design of the shear wall specimens, an evaluation of their failure is conducted, and the load and displacement data are collected through the utilisation of Mechanical Testing and Simulation (MTS) technology [19, 20]. Test specimen PS-1 fails in a diagonal sliding mode, while test specimen PS-2 fails in a compression shear mode. When the displacement loading of specimen PS-1 reaches 1.3 mm, it enters the cracking stage. When the displacement load reaches 10.5 mm, the main crack begins to form, and the test ends when the displacement reaches 26.1 mm. When the displacement loading of specimen PS-2 reaches 1.7 mm, it enters the cracking stage. When the displacement load reaches 7.8 mm, the main crack begins to form, and the test ends when the displacement reaches 11.2 mm. Fig. 2 shows the failure phenomenon and crack distribution of specimens PS-1 and PS-2.

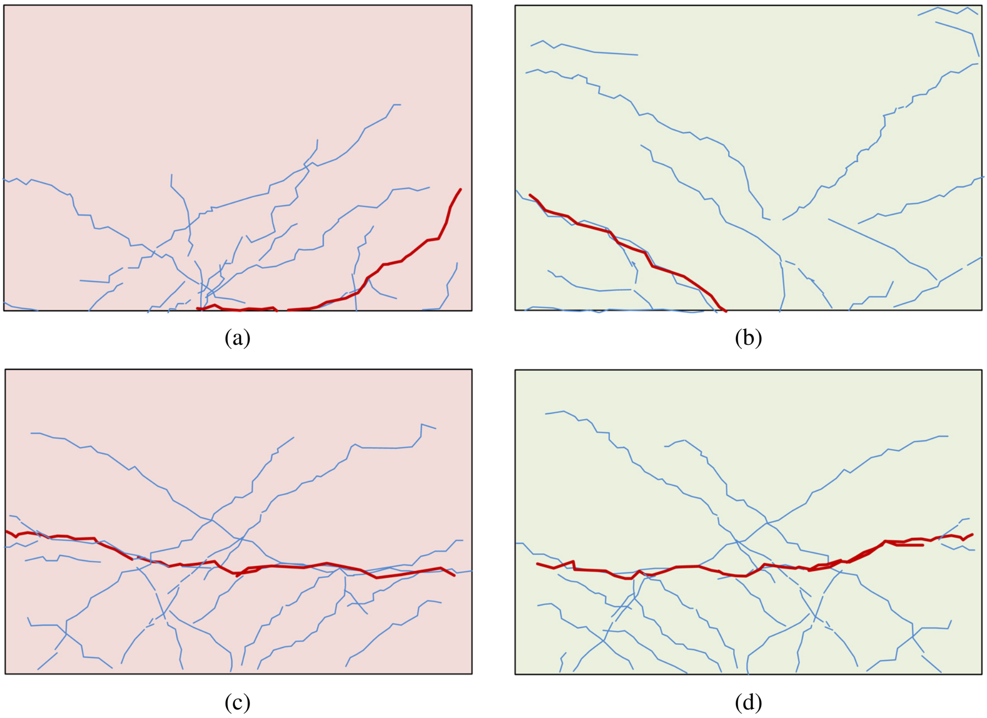

Fig. 2. Crack Distribution of PS-1 and PS-2 Specimens; (a) Distribution map of wall frontage cracks of PS-1, (b) Distribution map of wall reverse cracks of PS-1, (c) Distribution map of wall frontage cracks of PS-2, (b) Distribution map of wall reverse cracks of PS-2

PSSW contains the inner blade wall, the middle insulation layer, and the outer blade wall. Connectors play an important role in shear walls and also bear the design load [21, 22]. The outer blade plate of the sandwich shear wall is connected to the inner blade plate through connectors, which are subjected to vertical seismic effects, external blade plate loads, etc. The tension of the connecting components needs to consider wind loads and seismic effects [23]. The value of wind load is specified as the Load Code for Building Structures GB5009-2012, and the calculation equation is shown in Eq. (2.1).

$$\omega_k = \beta_{gz} \times \mu_s \times \mu_z \times \omega_o \tag{2.1}$$

In Eq. (2.1), ω_k – is the standard value of wind load acting on the exterior wall; β_{gz} – represents the gust coefficient; μ_s – represents the height variation coefficient of wind pressure; μ_z – represents the number of wind load shapes; ω_o – represents the basic wind pressure.

The calculation of earthquake action only needs to consider the two directions of tension perpendicular to the wall and shear parallel to the wall, as shown in Eq. (2.2).

$$P_{Ek} = \beta_E \times \alpha_{\max} \times G_K \tag{2.2}$$

In Eq. (2.2), P_{Ek} – represents seismic action; β_E – represents dynamic amplification factor; $\alpha_{\max}$ – represents the maximum value of horizontal seismic influence coefficient. connectors are designed by combining loads, parallel to the vertical load design of the layout as shown in Eq. (2.3).

$$S_V = 1.2G + 1.3P_{EK} \tag{2.3}$$

In Eq. (2.3), S_V – represents the surface area of the exterior wall; 1.2 represents the dynamic coefficient. The design equation for the horizontal load perpendicular to the layout is shown in Eq. (2.4).

$$S_h = 1.4\omega_k + 1.3P_{EK} \tag{2.4}$$

The displacement calculation of the connecting components is shown in Eq. (2.5) [24].

$$\begin{cases} d_A = d_d + \dfrac{2h_v}{3}\left[1 - \dfrac{d_d}{d_d + h_v}\right] \\ \Delta_A = \dfrac{V_d^3}{12nEI} \end{cases} \tag{2.5}$$

In Eq. (2.5), Δ – represents vertical displacement; V – represents the design value of vertical load on the outer blade wall; d_A – represents the calculated bending length of the connector; d_d – represents the thickness of the insulation layer; d_v – represents the anchorage length of the connector; E – represents the elastic modulus of the connector; I – represents the inertia moment of the connector interface. The experiment aims to explore the collaborative working mechanism of DRRBC's cast-in-place PSSW inner and outer blade shear walls by comparing the failure phenomena, energy dissipation capacity, and other indicators of sandwich shear walls and solid shear wall specimens.

2.2. Design of reinforced post pouring wet sandwich shear wall specimens

The connection methods and components of prefabricated structures play a crucial role in enhancing the seismic performance of sandwich shear walls and are key to improving construction efficiency. The assembly of monolithic concrete structures not only reduces labor requirements but also ensures high-quality components [25]. However, the existing connection methods and seismic performance of PSSW components are poor, leading to cracking and collapse of buildings. Therefore, this study proposes an improved CIP reinforced wet PSSW connection method. This method strengthens the strength of the post poured concrete with the original CIP concrete to achieve "equivalent CIP" PSSW. Two wall specimens are designed for the experiment, and the parameter design and detailed structure of the specimens are shown in Fig. 3. Among them, WS-1 is the reinforced post poured wet sandwich shear wall specimen of DRRBC, and WS-2 is the post poured sandwich shear wall specimen of DRRBC.

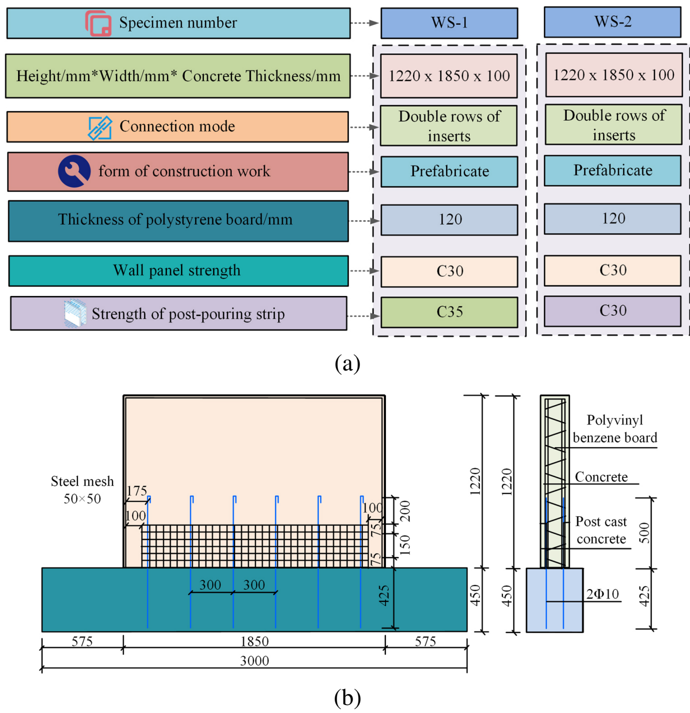

Fig. 3. Design parameters and detailed structure diagram of cast shear wall specimen; (a) Parameters of post-cast shear wall specimen, (b) Detailed construction diagram of WS-1 and WS-2

MTS built-in sensors are used to collect horizontal loads and real-time displacements of specimens. The failure mode of specimen WS-1 and WS-2 are single-sided compression shear and shear slip of the poured strip and prefabricated wall. When the displacement load of specimen WS-1 reaches 1.5 mm, it enters the cracking stage. When the displacement load reaches 9.4 mm, the main crack begins to form, and the test ends when the displacement reaches 24.8 mm. When the displacement load of specimen WS-2 reaches 1.2 mm, it enters the cracking stage. When the displacement load reaches 5.4 mm, the main crack begins to form, and the test ends when the displacement reaches 25.0 mm. The failure phenomenon and crack distribution of specimens WS-1 and WS-2 are shown in Fig. 4.

For the experimental setup and loading system, this study applies MTS actuators to sandwich shear walls. The experiment places steel pads on both sides of the top of the wall to avoid crushing local loading points, and fixed them with strong steel beams and anchor bolts [26]. The loading of horizontal loads is controlled by amplitude displacement. The loading of horizontal loads is controlled by amplitude displacement. The vertical load is applied by a 1000 kN jack through sensor control. This study uses a static acquisition system to evaluate changes in load values. The loading process is shown in Eq. (2.6).

$$n = \frac{N}{f_c bh} \tag{2.6}$$

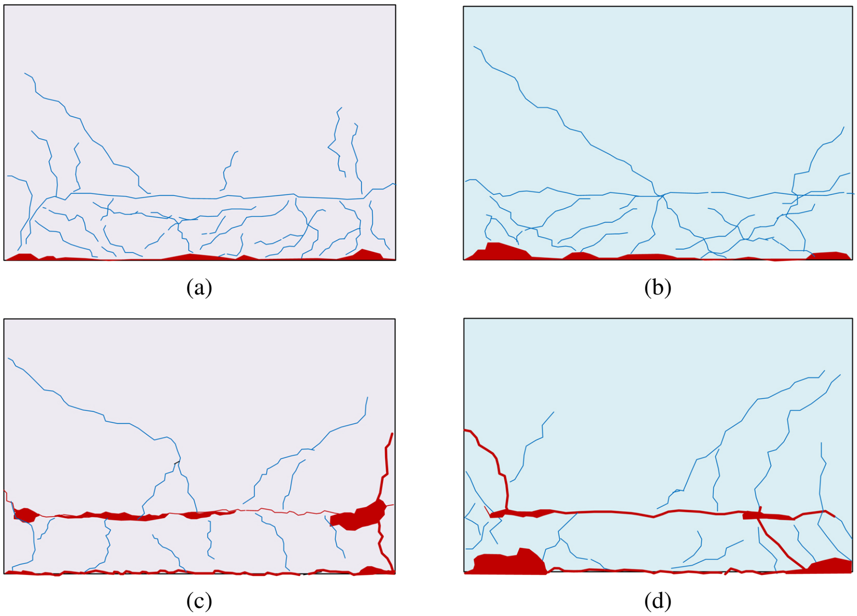

Fig. 4. Crack distribution of WS-1 and WS-2 specimens; (a) Distribution map of wall frontage cracks of WS-1, (b) Distribution map of wall reverse cracks of WS-1, (c) Distribution map of wall frontage cracks of WS-2, (b) Distribution map of wall reverse cracks of WS-2

In Eq. (2.6), n – is the axial compression ratio; f_c – is the compressive strength; b – is the PSW thickness; N – is the vertical axial pressure of the PSW component; h – is the PSW width. The experimental loading device is shown in Fig. 5.

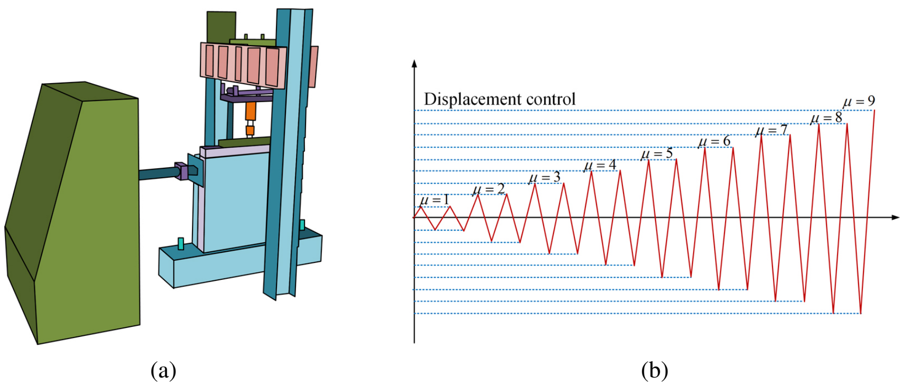

Fig. 5. Loading device and loading system diagram; (a) Loading device diagram, (b) Loading regime diagram

To test the compression of PSSW steel bars and concrete, the normal section bearing capacity of the shear wall was calculated in the experiment, as shown in Eq. (2.7).

$$\sigma^{+}_{\max} = f_t \tag{2.7}$$

In Eq. (2.7), $\sigma^{+}_{\max}$ – represents the edge stress; f_t – represents the tensile strength of concrete. Due to the linear increase in displacement and load caused by wall cracking, the calculation of CIP specimens is shown in Eq. (2.8).

$$F_{cr} = \left(f_t + \frac{N}{A}\right)\frac{Bh^2}{6H} \tag{2.8}$$

In Eq. (2.8), F_{cr} – represents the cracking load; A – represents the cross-sectional area; B – represents the cross-sectional width; h – represents the cross-sectional height. The calculation of the bending capacity of the normal section does not consider the stress of the steel bars within 1.5 times the height of the compression zone. The calculation equation for the height of the compression zone of the specimen under equilibrium conditions is shown in Eq. (2.9).

$$\begin{cases} \sum N = 0 \\ N = \alpha_1 \beta_1 f_c bx - f_{yw} A_{sw} \frac{h_{w0} - 1.5x}{h_{w0}} \end{cases} \tag{2.9}$$

In Eq. (2.9), α_1 – is the ratio of stress to the design value of concrete axial tensille strength; β_1 – is the stress graph conversion coefficient; b – is the wall width; x – is the height of the compression zone; h_{w0} – is the effective height of the wall section; f_{yw} – is the measured value of longitudinal steel bar tensile strength; A_{sw} – is the total area of longitudinal steel bars. The calculation equation for the distance between the edge tension sidesteel bars is shown in Eq. (2.10).

$$\begin{cases} \sum M = 0 \\ M = \alpha_1 \beta_1 f_c bx \left(h_{w0} - \frac{x}{2}\right) - f_{yw} A_{sw} \frac{(h_{w0} - 1.5x)^2}{2h_{w0}} - N\left(h_{w0} - \frac{h}{2}\right) \end{cases} \tag{2.10}$$

In Eq. (2.10), M – is the bending moment at the bottom of the wall. The calculation equation for the horizontal bearing capacity of the specimen is shown in Eq. (2.11).

$$V = \frac{M}{h_0} \tag{2.11}$$

In Eq. (2.11), V – represents the horizontal bearing capacity; h_0 – represents the distance from the bottom of the wall to the loading end.

3. Results

This section first compared and analyzed sandwich shear walls and solid shear walls based on CIP connections, exploring the collaborative working mechanism of the inner and outer leaf walls of the shear wall. This study compared different specimens through quasi-static testing to explore the seismic effect of improving the shear wall connection method.

3.1. Analysis of the collaborative work of PSSW inner and outer leaf walls with cast in place connection

The experiment used MTS technology to collect the load and displacement of PSW specimens. By comparing and analyzing the hysteresis curve, skeleton curve, stiffness degradation curve, and other indicators of CIP double row reinforced sandwich and solid shear wall specimens, the coordinated operation of the inner and outer blades of the sandwich shear wall could be achieved.

In Fig. 6, the hysteresis curves and skeleton curves of CIP double row reinforced sandwich and solid shear wall specimens were compared and analyzed. In Fig. 6a, when the displacement of specimen PS-1 was loaded to 1.3 mm, the horizontal load was 87.57 kN. When the displacement was loaded to 10.5 mm, the horizontal load was 222.58 kN, and the main crack was formed as a result. When the displacement load of specimen PS-2 reached 1.7 mm, the horizontal load was 72.52 kN. As the displacement load was 7.8 mm, the horizontal load was 275.45 kN, meanwhile the main crack of the specimen had formed. In Fig. 6b, before the formation of cracks, the skeleton curve of the specimen was roughly straight, and after the formation of cracks, the curve showed a turning point. When the displacement of specimen PS-1 reached 10.5 mm, the skeleton curve showed a relatively flat trend. After the displacement of specimen PS-2 reached 7.8 mm, the skeleton curve showed a turning point, and its bearing capacity significantly decreased, indicating that the specimen had strong destructive performance.

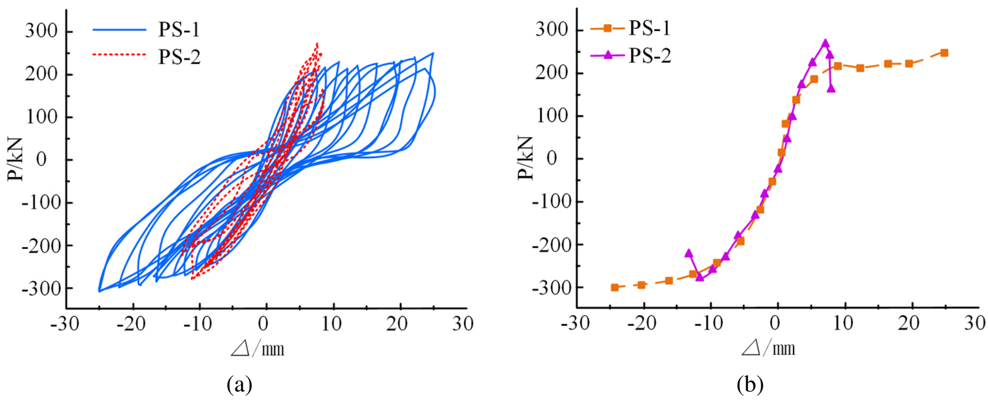

Fig. 6. Hysteretic curves and skeleton curves of PS-1 and PS-2 specimens; (a) The hysteresis curves of PS-1 and PS-2 samples, (b) Specimen PS-1 and PS-2 skeleton curves

In Fig. 7, to further compare the performance of the specimens, the cracking, peak value, and failure load of the specimens were extracted and the average skeleton curve and normalized skeleton curve were compared. When the displacement of specimen PS-1 reachesd 1.3 mm, the cracking load was 62.46 kN; When the displacement was 10.5 mm, the peak load was

222.58 kN; When the displacement reached 26.1 mm, the destructive load reached 258.25 kN. When the displacement of specimen PS-2 was 1.7 mm, the cracking load was 62.46 kN; When the displacement was 7.8 mm, the peak load reached 275.45 kN; When the displacement reached 11.2 mm, the failure load decreased to 189.56 kN. The failure load of specimen PS-1was 195.79 kN higher than the cracking load, 35.67 kN higher than the peak load, and the load displacement was reduced by 15.6 mm. The failure load of specimen PS-2 was only 127.1 kN higher than the cracking load, and 85.89 kN lower than the peak load, with a load displacement reduction of 3.4 mm. Therefore, the PS-1's cracking load and peak load were lower than PS-2, indicating that PS-1 had better ductility.

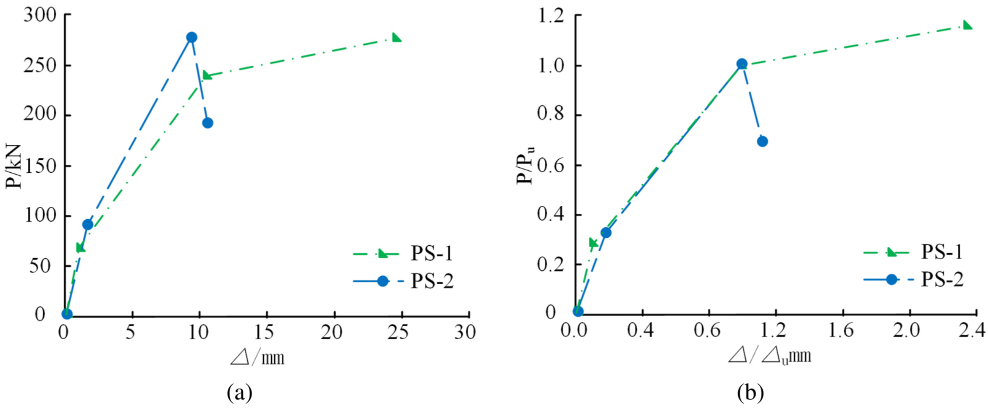

Fig. 7. Average and normalized skeleton curves of PS-1 and PS-2 specimens; (a) Average skeleton curves of PS-1 and PS-2 specimens, (b) Normalized skeleton curves of PS-1 and PS-2 specimens

The stiffness degradation curves, capacity dissipation coefficients, and Equivalent Viscous Damping Coefficients (EVDC) of specimens PS-1 and PS-2 were compared. In Fig. 8a, when the displacement of specimen PS-1 increased from 1.3 to 10.5 mm, the stiffness of the specimen decreased from 75.21 kN to 22.3 kN. After the displacement reached 10.5 mm, the stiffness degradation slowly decreased. Due to the rapid formation of the main crack, the stiffness of specimen PS-2 decreased rapidly, from 60.4 kN to 18.5 kN. In Fig. 8b, PS-1-E and PS-2-E represent capacity dissipation coefficients of specimen PS-1 and PS-2 respectively, and PS-1-h and PS-2-h represent the EVDC of specimen PS-1 and PS-2 respectively. The results showed that the EVDC of specimen PS-1 under cracking, peak, and failure loads were 0.056, 0.110, and 0.151, respectively; The EVDC of specimen PS-2 were 0.052, 0.062, and 0.090, respectively, all lower than specimen PS-1. The energy dissipation coefficients of specimen PS-1 were 0.366, 0.557, and 0.940, respectively. Therefore, the stiffness degradation performance and energy dissipation capacity of specimen PS-1 were superior, which proved that the inner and outer blades of the sandwich shear wall worked well together.

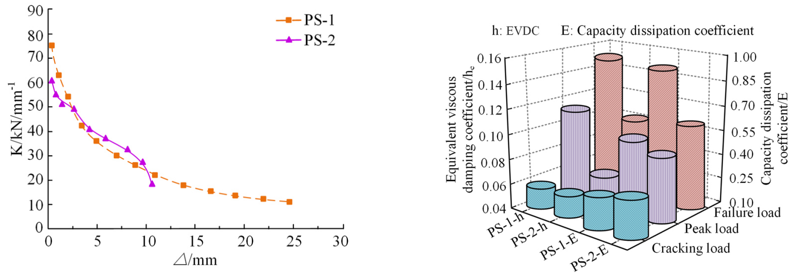

(a) (b)

Fig. 8. Stiffness degradation curves, capacity dissipation coefficients and EVDC of PS-1 and PS-2 specimens; (a) Stiffness degradation curves of PS-1 and PS-2 specimens, (b) Capacity dissipation coefficient and equivalent viscous damping coefficient of PS-1 and PS-2 specimens

3.2. Seismic performance testing of reinforced wet shear walls with DRRBC

In Fig. 9, to investigate the seismic performance of PSSW with post cast wet connections, the seismic performance indicators of DRRBC CIP specimens, reinforced post cast wet specimens, and unreinforced post cast wet specimens were compared. In Fig. 9a, when the displacement of specimen WS-1 reached 1.5 mm, the load was 87.24 kN, and its hysteresis curve increased linearly. When the displacement was loaded to -9.4 mm, the load was 239.12 kN, and the hysteresis curve gradually showed an S-shape. With the loading of displacement, the hysteresis loop peak increased nonlinearly. When the displacement was loaded to 13.2 mm, the load reached up to 285.46 kN. In Fig. 9b, when the displacement load of specimen WS-2 reached 1.2 mm, the load was 83.26 kN, and its hysteresis curve showed a shuttle shape. When the displacement was loaded to -5.4 mm, the load was 125.66 kN, and the displacement loading caused the hysteresis peak to increase nonlinearly. When the displacement reached 7.8 mm, the horizontal load reached 245.55 kN. With the loading of displacement, the hysteresis loop bearing capacity of prefabricated walls increased, resulting in a decrease in the bearing capacity of the specimens. The peak load and hysteresis area of specimen WS-1 were both greater than those of specimen WS-2.

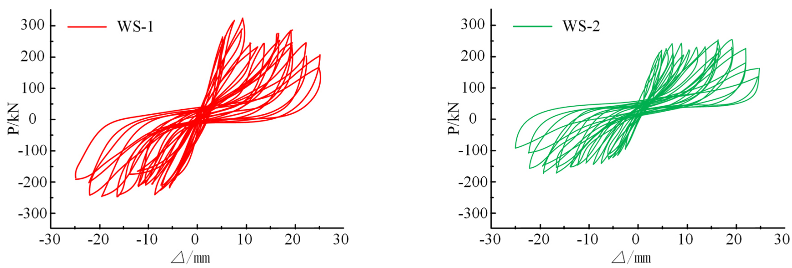

(a) (b)

Fig. 9. Hysteresis curves of specimen WS-1 and WS-2; (a) The hysteresis curves of WS-1 samples, (b) The hysteresis curves of WS-2 samples

In Fig. 10, the skeleton curves and stiffness degradation curves of specimens PS-1, WS-1, and WS-2 were analyzed. In Fig. 10a, when the displacement of specimen WS-1 was loaded to 9.4 mm, its peak load reached 301.25 kN. After a displacement of 9.4 mm, the skeleton curve showed a phenomenon of first decreasing and then increasing, with the load decreasing to 251.23 kN and then increasing to 284.56 kN. After the displacement of specimen WS-2 was loaded to 7.8 mm, the skeleton curve showed a smooth trend. When the displacement load reached 20.1 mm, the load reached its peak at 245.55 kN, and the skeleton curve slowly decreased. In Fig. 10b, the initial stiffness of specimens WS-1, PS-1, and WS-2 were 80.12 kN, 75.21 kN, and 68.54 kN, respectively. The secant stiffness of specimen WS-1 was higher than that of specimens WS-2 and PS-1 before a displacement of 10.3 mm, and the stiffness value was 25.12 kN. When the displacement reached 10.3 mm, the stiffness of all three specimens slowly decreased, and the decreasing trend was consistent. This result proved that the seismic performance of shear walls with post poured wet connections was better.

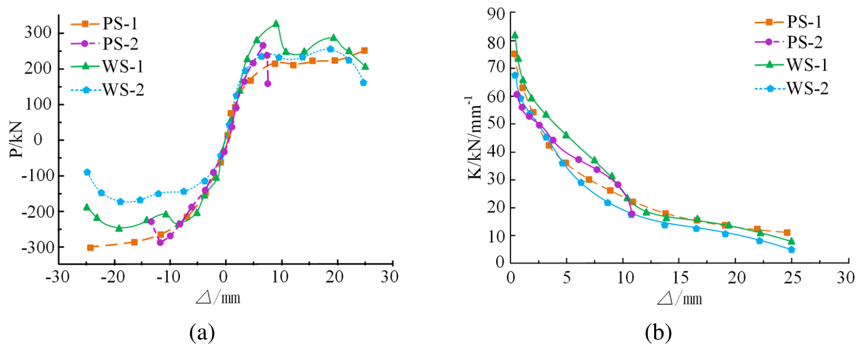

Fig. 10. Comparison of skeleton curves and stiffness degradation curves of PS-1, PS-2, WS-1 and WS-2 specimens; (a) Skeleton curves of specimens PS-1, PS-2, WS-1 and WS-2, (b) Stiffness degradation curves of specimens PS-1, PS-2, WS-1 and WS-2

In Fig. 11, the averaged skeleton curves and normalized skeleton curves of specimens PS-1, WS-1, and WS-2 were compared. When the displacement of specimen PS-1 reached 1.3 mm, the cracking load was 62.46 kN; When the displacement was 10.5 mm, the peak load was 222.58 kN; When the displacement reached 26.1 mm, the destructive load reached 258.25 kN. When the displacement of specimen WS-1 was 1.5 mm, the cracking load was 87.24 kN; When the displacement was 13.2 mm, the peak load reached 290.46 kN; When the displacement reached 26.1 mm, the failure load decreased to 163.18 kN. When the displacement of specimen WS-2 was 1.2 mm, the cracking load was 83.26 kN; When the displacement was 17.8 mm, the peak load reached 201.37 kN; When the displacement reached 26.1 mm, the failure load decreased to 121.58 kN. The failure load of specimen WS-1 was 75.94 kN higher than the cracking load, 167.28 kN lower than the peak load, and the load displacement was reduced by 12.9 mm. The failure load of specimen WS-2 was only 38.32 kN2 higher than the cracking load, and 79.79 kN lower than the peak load, with a load displacement reduction of 8.3 mm. Compared with specimen WS-2, specimen WS-1 had better ductility. The results further demonstrated the superiority of the wet connection method after pouring.

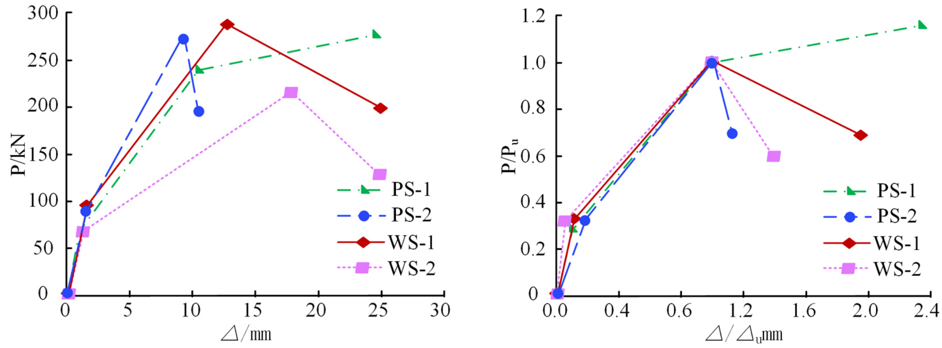

(a) (b)

Fig. 11. Comparison of mean and normalized skeleton curves of PS-1, PS-2, WS-1, and WS-2 specimens; (a) Average skeleton curves of specimens PS-1, PS-2, WS-1 and WS-2, (b) Normalized skeleton curves of specimens PS-1, PS-2, WS-1 and WS-2

In Fig. 12, the capacity dissipation coefficients and EVDC of specimens PS-1, WS-1, and WS-2 were compared. In Fig. 12a, the EVDC of specimen PS-1 under cracking, peak, and failure loads were 0.056, 0.110, and 0.151, respectively. The EVDC of WS-1 were 0.042, 0.077, and 0.122; The WS-2 values were 0.066, 0.090, and 0.137. In Fig. 12b, the energy dissipation coefficients of specimen PS-1 under cracking, peak, and failure loads were 0.366, 0.557, and 0.940, respectively. The energy dissipation coefficients of specimen WS-1 were 0.366, 0.557, and 0.940; The WS-2 values were 0.366, 0.702, and 0.940. The energy dissipation capacity of specimen WS-1 was better than PS-1 and WS-2, which proved that the shear wall with reinforced wet connection had stronger seismic resistance and better seismic effect.

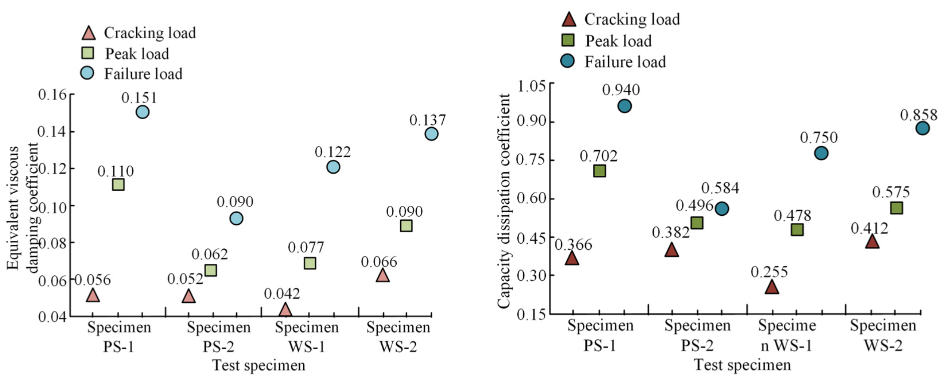

(a) (b)

Fig. 12. Comparison of Seismic Performance Indexes of Different Specimens; (a) Equivalent viscous damping coefficient of PS-1, PS-2 WS-1 and WS-2 specimens, (b) Capacity dissipation coefficient of PS-1, PS-2 WS-1 and WS-2 specimens

4. Discussion and conclusions

This study improves the single row plug-in bar connection method with poor seismic performance, designs a CIP connection method based on double row plug-in bars, and proposes a PSSW with reinforced wet connection after pouring. When the displacement of specimen PS-1 was loaded to 10.5 mm, the horizontal load was 222.58 kN. When the displacement of specimen PS-2 reached 7.8 mm, the horizontal load was 275.45 kN. The cracking load of specimen PS-1 was 28.10% of the peak load, and the displacement in the failure state was 2.49 times that of the peak load displacement. The EVDC under cracking, peak, and failure loads were 0.056, 0.110, and 0.151, respectively; The energy dissipation coefficients were 0.366, 0.557, and 0.940, respectively. The EVDC of specimen PS-2 were 0.052, 0.062, and 0.090, respectively. When the displacement of specimen WS-1 based on post pouring wet connection reached 13.2 mm, the load reaches up to 285.46 kN. The secant stiffness of specimen WS-1 was higher than that of specimens WS-2 and PS-1 before a displacement of 10.3 mm, and the stiffness value was 25.12 kN. The peak load of specimen WS-1 was 3.33 times the cracking load, and the peak load of specimen WS-2 was 2.42 times the cracking load. The displacement of the failure load of specimen WS-1 was 12.9 mm more than the peak load displacement, while the displacement of the failure load of specimen WS-2 was only 8.3 mm more than the peak load displacement. The energy dissipation coefficients of specimen WS-1 were 0.366, 0.557, and 0.940, respectively. The dissipation coefficients of WS-2 were 0.366, 0.702, and 0.940, respectively. The reinforced wet connection shear wall has strong seismic resistance and better seismic effect. This study did not consider the influence of concrete thickness and the distance between shear wall connectors on the seismic performance of PSSW, and further research is needed to investigate this. https://doi.org/

References

[1] Q. Liu, W. Liang, C. Chan, Y. Cao, and M. Lu, "The impact of low-carbon policy on green manufacturing development", *Indoor and Built Environment*, vol. 32, no. 8, pp. 1606–1620, 2023, doi: 10.1177/1420326X221121061.

[2] X. Li, C. Wang, M.A. Kassem, H.H. Alhajlah, and S. Bimenyimana, "Evaluation method for quality risks of safety in prefabricated building construction using SEM-SDM approach", *International Journal of Environmental Research and Public Health*, vol. 19, no. 9, art. no. 5180, 2022, doi: 10.3390/ijerph19095180.

[3] J. Akor, L. Onjefu, J. Edeh, and A. Olubambi, "Suitability of Crushed Sandcrete Block (CSB) as a partial replacement for fine aggregate in concrete structures", *Archives of Advanced Engineering Science*, vol. 1, no. 1, pp. 10–19, 2023.

[4] I. Ahmad and M. Shokouhian, "Promoting sustainable green infrastructure: Experimental and numerical investigation of concrete reinforced with recycled steel fibers", *Archives of Advanced Engineering Science*, vol. 3, no. 4, pp. 252–264, 2024, doi: 10.47852/bonviewAAES42022837.

[5] A. Saeed, H.M. Najm, A. Hassan, S. Qaidi, M.M.S. Sabri, and N.S. Mashaan, "A comprehensive study on the effect of regular and staggered openings on the seismic performance of shear walls", *Buildings*, vol. 12, no. 9, art. no. 1293, 2022, doi: 10.3390/buildings12091293.

[6] C. Mei, Z. Zhao, Y. Zhang, D. Wang, and C. Wu, "Performance evaluation and shear resistance of modular prefabricated two-side connected composite shear walls", *KSCE Journal of Civil Engineering*, vol. 25, no. 8, pp. 2936–2950, 2021, doi: 10.1007/s12205-021-2394-6.

[7] I. Ćurković, I. Lukačević, V. Žuvelek, and A. Rajić, "Numerical investigation of shear connection in cold-formed steel-concrete composite beam", *Proceedings in Civil Engineering*, vol. 5, no. 4, pp. 847–856, 2022, doi: 10.1002/cepa.1827.

[8] Y. Shen, M. Xu, Y. Lin, C. Cui, X. Shi, and Y. Liu, "Safety risk management of prefabricated building construction based on ontology technology in the BIM environment", *Buildings*, vol. 12, no. 6, art. no. 765, 2022, doi: 10.3390/buildings12060765.

[9] Q. Wang, W. Guo, X. Xu, R. Deng, X. Ding, and T. Chen, "Analysis of carbon emission reduction paths for the production of prefabricated building components based on evolutionary game theory", *Buildings*, vol. 13, no. 6, art. no. 1557, 2023, doi: 10.3390/buildings13061557.

[10] Y. Xiao, Z. Wu, and Y. Gong, "Study on alkali-activated prefabricated building recycled concrete powder for foamed lightweight soils", *Materials*, vol. 16, no. 11, art. no. 4167, 2023, doi: 10.3390/ma16114167.

[11] Y. Zhao, C. Cao, Z. Liu, and E. Mu, "Intelligent control method of hoisting prefabricated components based on Internet-of-Things", *Sensors*, vol. 21, no. 3, art. no. 980, 2021, doi: 10.3390/s21030980.

[12] Q. Han, J. Chang, G. Liu, and H. Zhang, "The carbon emission assessment of a building with different prefabrication rates in the construction stage", *International Journal of Environmental Research and Public Health*, vol. 19, no. 4, art. no. 2366, 2022, doi: 10.3390/ijerph19042366.

[13] B. Zhao, L. Du, G. Chen, L. Yue, C. Cui, and M. Ge, "Experimental and numerical study on the shear performance of stainless steel-GFRP connectors for use in precast concrete sandwich panels", *Scientific Reports*, vol. 14, art. no. 13814, 2024, doi: 10.1038/s41598-024-64543-1.

[14] Y.L. Liu, C. Liu, H. Pan, J.L. Fu, J.Q. Huang, and J.Q. Hong, "Experimental and numerical investigation on seismic performance of semi-precast concrete sandwich shear wall", *Advances in Structural Engineering*, vol. 25, no. 13, pp. 2772–2784, 2022, doi: 10.1177/13694332221108435.

[15] H. Tawil, C.G. Tan, N.H. Ramli Sulong, F.M. Nazri, M.F. Shamsudin, and N. Muhamad Bunnori, "Optimization of shear resistance in precast concrete sandwich wall panels using an S-type shear connector", *Buildings*, vol. 14, no. 6, art. no. 1725, 2024, doi: 10.3390/buildings14061725.

[16] G. Xu, T. Guo, and A. Li, "Seismic performance and fragility analysis of precast concrete sandwich wall structure", *Journal of Earthquake Engineering*, vol. 27, no. 2, pp. 410–433, 2023, doi: 10.1080/13632469.2021.2003272.

[17] D. Chen, K. Li, Z. Yuan, B. Cheng, and X. Kang, "Shear behavior of FRP connectors in precast sandwich insulation wall panels", *Buildings*, vol. 12, no. 8, art. no. 1095, 2022, doi: 10.3390/buildings12081095.

[18] S. Mahmoud, "In-plane shear-wall configuration effects on the seismic performance of symmetrical multistory reinforced-concrete buildings", *International Journal of Civil Engineering*, vol. 19, no. 10, pp. 1195–1208, 2021, doi: 10.1007/s40999-021-00634-8.

[19] R. Jasiński and K. Grzyb, "Adaptation of the total stiffness method to the load distribution of stiffening masonry walls according to Eurocode 6", *Archives of Civil Engineering,* vol. 68, no. 1, pp. 255-274, 2022, doi: 10.24425/ace.2022.140167.

[20] T.S. Fawale, J.O. Dada, O. Olamilokun, and O. Alimi, "Responsiveness of construction participants to building collapse in Lagos state, Nigeria", *Engineering Heritage Journal*, vol. 7, no. 1, pp. 1–9, 2023, doi: 10.26480/gwk.01.2023.01.09.

[21] A.D. Almutairi, Y. Bai, and W. Ferdous, "Flexural behaviour of GFRP-softwood sandwich panels for prefabricated building construction", *Polymers*, vol. 15, no. 9, art. no. 2102, 2023, doi: 10.3390/polym15092102.

[22] A.A. Ayu Oka Saraswati, I.B.G. Primayatna, I.B.G. Darmayasa, and P. Suardana, "Artistic acoustic panel recycled material from plastic bottles and waste of Sampyan, sawdust, husks, straw", *Engineering Heritage Journal*, vol. 5, no. 2, pp. 42–44, 2021, doi: 10.26480/gwk.02.2022.42.44.

[23] M. AlHamaydeh, M. Elkafrawy, and S. Banu, "Seismic performance and cost analysis of UHPC tall buildings in UAE with ductile coupled shear walls", *Materials*, vol. 15, no. 8, art. no. 2888, 2022, doi: 10.3390/ma15082888.

[24] C. Li, J. Wu, J. Zhang, and C. Tong, "Elastic displacement spectrum-based design approach for precast concrete frame with replaceable energy-dissipating connectors", *Journal of Earthquake Engineering*, vol. 26, no. 5, pp. 2411–2436, 2022, doi: 10.1080/13632469.2020.1762805.

[25] X. Zhang, S. Xu, and S. Li, "Study on shear performance of cold-formed thin-walled steel-paper straw board composite wall with openings", *Archives of Civil Engineering*, vol. 69, no. 1, pp. 571–591, 2023, doi: 10.24425/ace.2023.144189.

[26] W. Ampadu, H. Malik, R. Diezmos, and J. Hyslob, "Safety system design and overfill protection for loading asphalt onto trucks", *Systems Engineering*, vol. 25, no. 4, pp. 387–403, 2022, doi: 10.1002/sys.21620.

Received: 2024-09-25, Revised: 2024-12-02